Neuroanatomical pathways of TMS therapy for depression

Caio Seguin[1,2,†], Sina Mansour L.[3], Richard F. Betzel[4,5], Evgeny J. Chumin[6,7,8], Maria Grazia Puxeddu[9], Jinglei Lv[10], Linden Parkes[11], Luca Cocchi[12,13], Paul B. Fitzgerald[14,15], Robin F. H. Cash[1,16,*] & Andrew Zalesky[1,16,*]

1. Systems Lab, Department of Psychiatry, The University of Melbourne, Melbourne, Victoria, Australia
2. Indiana University, Department of Psychological and Brain Sciences, Bloomington, IN, USA
3. Centre for Sleep & Cognition & Centre for Translational Magnetic Resonance Research, Yong Loo Lin School of Medicine, National University of Singapore, Singapore
4. University of Minnesota, Department of Neuroscience, Minneapolis, MN, USA
5. Masonic Institute for the Developing Brain, Minneapolis, MN, USA
6. Indiana University Alzheimer's Disease Research Center, Indiana University School of Medicine (IUSM), Indianapolis, IN, USA
7. Center for Neuroimaging, IUSM, Indianapolis, IN, USA
8. Medical Imaging Research Center, Department of Radiology and Imaging Sciences, IUSM, Indianapolis, IN, USA
9. Department of Computer, Control, and Management Engineering, University of Rome La Sapienza, Rome, Italy
10. School of Biomedical Engineering & Brain and Mind Centre, The University of Sydney, Sydney, Australia
11. Department of Psychiatry, Rutgers University, Piscataway, NJ, USA
12. QIMR Berghofer Medical Research Institute, Brisbane, Queensland, Australia
13. Faculty of Medicine, School of Biomedical Sciences, University of Queensland, Brisbane, Queensland, Australia
14. School of Medicine and Psychology, College of Health and Medicine, The Australian National University, Canberra, ACT, Australia
15. Monarch Research Institute, Monarch Mental Health Group, Melbourne, Victoria, Australia
16. Department of Biomedical Engineering, Faculty of Engineering and Information Technology, The University of Melbourne, Melbourne, Victoria, Australia

† Corresponding author (caio.seguin@unimelb.edu.au)
* Authors contributed equally

Abstract

TMS therapy for depression delivered to the dorsolateral prefrontal cortex (DLPFC) aims to modulate activity in the subgenual cingulate cortex (SGC). However, these regions lack direct axonal connections, and the neuroanatomical mechanisms underlying the therapy's efficacy remain unknown. Here, we use connectome modelling to map polysynaptic fibre pathways from the DLPFC to the SGC that are associated with TMS treatment response in depression. We show that polysynaptic communication through the structural connectome is correlated with treatment response in two independent cohorts of patients treated with TMS to the left DLPFC ($r = -0.56$, $p = 0.0018$; $r = -0.52$, $p = 0.0047$), and that DLPFC sites of stronger negative functional connectivity to the SGC are connected to it via shorter fibre pathways. Our results shed light onto the neuroanatomical basis of TMS therapy for depression and pave the way for brain stimulation protocols based on polysynaptic communication via the connectome.

Main text

Transcranial magnetic stimulation (TMS) of the left dorsolateral prefrontal cortex (DLPFC) is a therapy for refractory depression [1]. The therapy's efficacy is thought to relate to indirect modulation of the subgenual cingulate cortex (SGC)—a structure that is not directly accessible to TMS. Support for this comes from observations that stimulating the DLPFC elicits acute and lasting changes in SGC activity and connectivity, as demonstrated by TMS combined with functional magnetic resonance imaging (fMRI) [2–4] and intracranial recordings [5]. Moreover, multiple fMRI studies indicate that baseline functional connectivity (FC) between DLPFC TMS sites and the SGC predicts patient treatment responses [6–9].

Interestingly, direct white matter fibres between the DLPFC and the SGC do not exist. Tract-tracing work in rhesus monkeys reports absent axonal projections between the two regions [10,11], while human brain imaging has not identified tracts that could establish a direct communication channel from the DLPFC to the SGC [12]. The propagation of DLPFC stimulation to the SGC is therefore hypothesized to be polysynaptic, i.e., mediated by a sequence of intermediate regions interlinked via white matter connectivity. Current methods to map the white matter circuits using brain stimulation are limited to direct, "one-hop" fibres between anatomically connected regions [13,14], making them unsuitable to understand DLPFC-SGC communication [15]. As a result, despite the progress achieved using fMRI, the neuroanatomical circuits mediating the therapeutic outcomes of TMS in depression remain elusive. This knowledge gap poses a central barrier to understanding and leveraging the role of the human structural connectome in mediating the response to TMS therapy.

Here, we use advances in connectome modelling to map polysynaptic fibre pathways from the DLPFC to the SGC and show that they explain TMS antidepressant effects. Network communication models quantify the capacity of signal transmission between regions via the connectome (Fig 1A) [16,17]. The models can identify multi-hop pathways (sequences of two or more white matter tracts) between grey matter structures that are not connected by a direct fibre. We use this modelling framework to reveal putative neuroanatomical routes traversed by TMS in two depression cohorts.

We consider two independent cohorts of individuals with treatment resistant depression who underwent repetitive TMS to the left DLPFC (Cohort I: $N = 25$, 17 females, 54.8 ± 9.9 years old [7]; Cohort II: $N = 24$, 10 females, 44.5 ± 11.8 years old [8]; *Materials and Methods*). Stimulation sites in the DLPFC were determined separately for each patient using established methods (Fig 1B,F). Treatment response was measured as the percentage change in the Montgomery–Åsberg Depression Rating Scale (cohort I) and Beck Depression Inventory (cohort II) scores before and after TMS therapy. We mapped polysynaptic white matter pathways from volumes of activated tissue centred at TMS coordinates in the left DLPFC to the right SGC (10-mm radius sphere centred at MNI [6,16,–10], as per [6–8]). Pathways were identified using the *shortest path routing* model, and a pathway's capacity to support TMS propagation was measured as its average number of hops through the connectome (i.e., number of white matter tracts traversed from the stimulation site to the SGC). Pathways were mapped on a normative connectome (*Materials and Methods*).

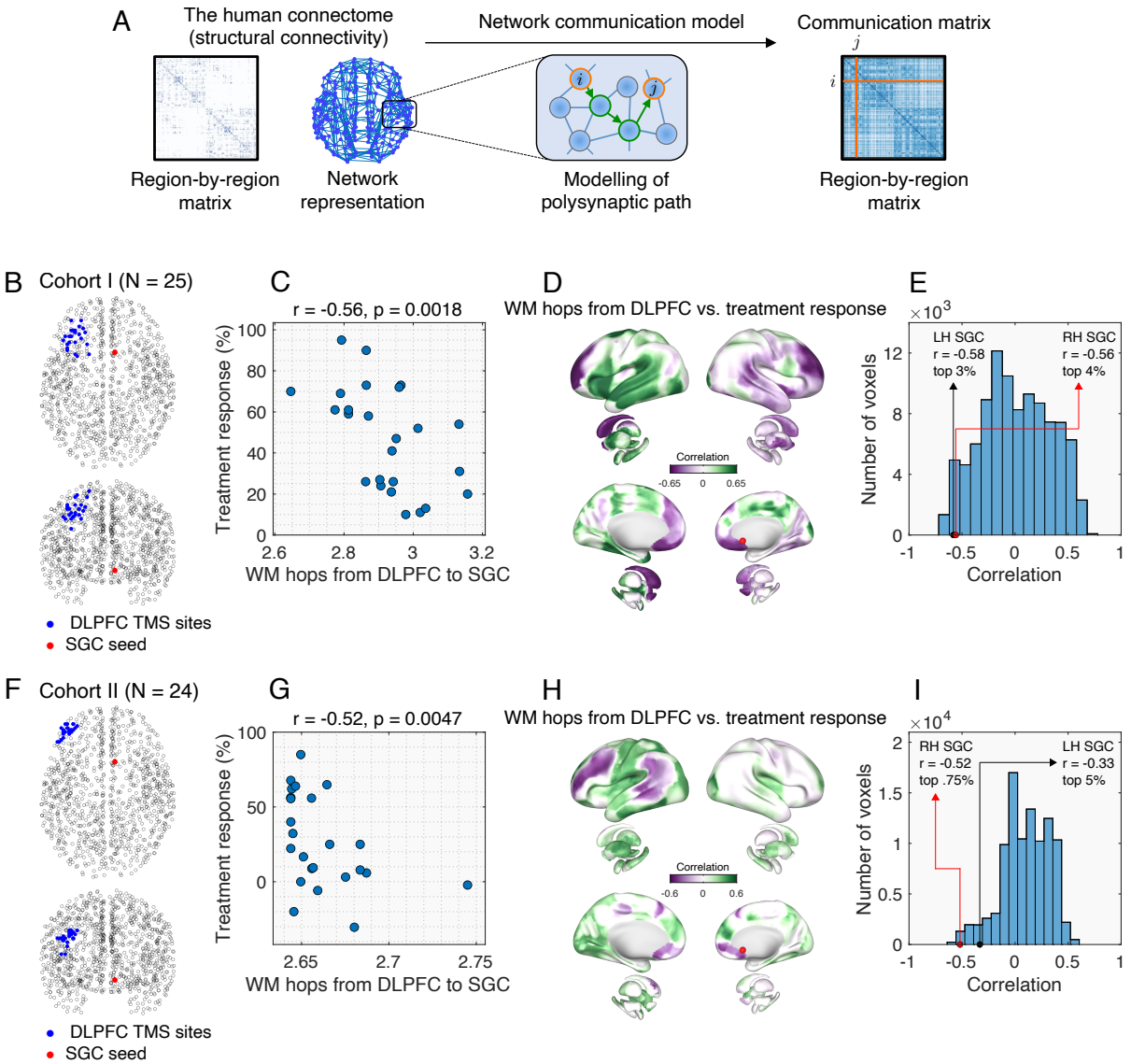

Figure 1. DLPFC-SGC white matter pathways were associated with TMS treatment response. **(A)** Network communication models quantify the capacity for signalling via the structural connectome. The models identify putative paths of polysynaptic communication between regions not connected by a direct fibre. **(B)** TMS and SGC coordinates in Cohort I. Black circles denote the grey matter regions of the connectome. **(C)** Relationship between treatment response and the number of white matter tracts traversed (WM hops) from DLPFC stimulation sites to the SGC, in Cohort I. **(D)** Cortical map of the correlation between WM hops from DLPFC stimulation sites and treatment response, in Cohort I. In purple (green) are downstream regions for which efficient communication from the DLPFC was associated with better (worse) clinical outcomes. Treatment response was prominently associated with fewer WM hops from DLPFC stimulation site to right SGC (red dot, MNI [6,16, –10]), while also highlighting other regions of potential interest. **(E)** Distribution of correlations shown in (D). **(F-I)** Same as B-E but in Cohort II.

We found that polysynaptic white matter pathways were associated with treatment response in both cohorts. Patients stimulated at DLPFC sites connected to the SGC by fewer white matter hops—shorter, more direct communication channels—showed higher rates of clinical improvement (cohort I: Spearman rank correlation coefficient $r = -0.56$, one-tailed $p = 0.0018$, Fig 1C; cohort II: $r = -0.52$, $p = 0.0046$, Fig 1G). This association was robust to leave-one-out outlier sensitivity tests in both cohorts (Fig S1). This suggests that white matter connectivity plays a key role in polysynaptic signalling from precise DLPFC stimulation sites to the SGC, and that variations in TMS coordinates—leading to differences in how efficiently signals are transmitted via the connectome—contribute to heterogeneity in patient outcomes.

While there is accumulating evidence implicating the right SGC in TMS therapy for depression [2–9], could modulation of other downstream regions be more relevant to treatment response? To investigate this, we computed white matter pathways not only to the SGC, but to 10-mm spheres centred at each grey matter voxels in the brain, yielding a whole-brain map of the correlation between TMS propagation and treatment response (Fig 1D,H). Strikingly, our analysis corroborates clinical reports on the importance of the SGC seed centred at MNI [6,16,–10] [6–9], with this coordinate positioned at the top 4.25% and 0.75% of most relevant voxels to patient outcomes in cohorts I and II (Fig 1E,I). The contralateral left SGC seed (MNI [6,16,10]) was similarly associated with treatment response in cohort I but yielded weaker correlations in cohort II, suggesting that the right SGC may be more consistently implicated with clinical outcomes [6,7]. We also note the presence of regions for which *longer* communication pathways were associated with better treatment response (e.g., left inferior temporal cortex), suggesting that dampening TMS modulation of certain areas may also contribute to treatment efficacy.

What neuroanatomical structures underpin TMS communication from the left DLPFC to the right SGC? To answer this question, we combined modelling results across individuals of the same cohort and counted the occurrences of the network paths used to infer white matter communication (Fig 2A,D). In agreement with evidence for the lack of direct DLPFC-SGC fibres [10,12], we found that all paths were formed by a sequence of at least 2 tracts, i.e., traversed at least one intermediate grey matter region (Fig 2B,E). In the first cohort, where TMS sites were spread across the posterior left DLPFC, communication was supported by distributed routes traversing the left caudate, right accumbens area, right superior frontal cortex, and right caudal anterior cingulate cortex (Fig 2C). The primary route was a subcortical pathway comprising three hops via the connectome: from stimulation sites in the left DLPFC to the left caudate, to the right accumbens area via the anterior commissure, to the right SGC via short range fibres (Fig 2G). A complementary cortical pathway was also composed of three hops: from stimulation sites to homotopic prefrontal areas via the corpus callosum, to the right caudal anterior cingulate cortex, to the SGC (Fig 2H). In the second cohort, where stimulation sites were circumscribed to a smaller frontal part of the left DLPFC, routes were less diverse and directed almost exclusively through the subcortex (Fig 2F). The primary pathway in this cohort was the same as in the previous one, i.e., three hops via the left caudate and right accumbens area. We also observed a secondary pathway comprising only two hops, where the left caudate was the sole mediator between stimulation sites and the SGC.

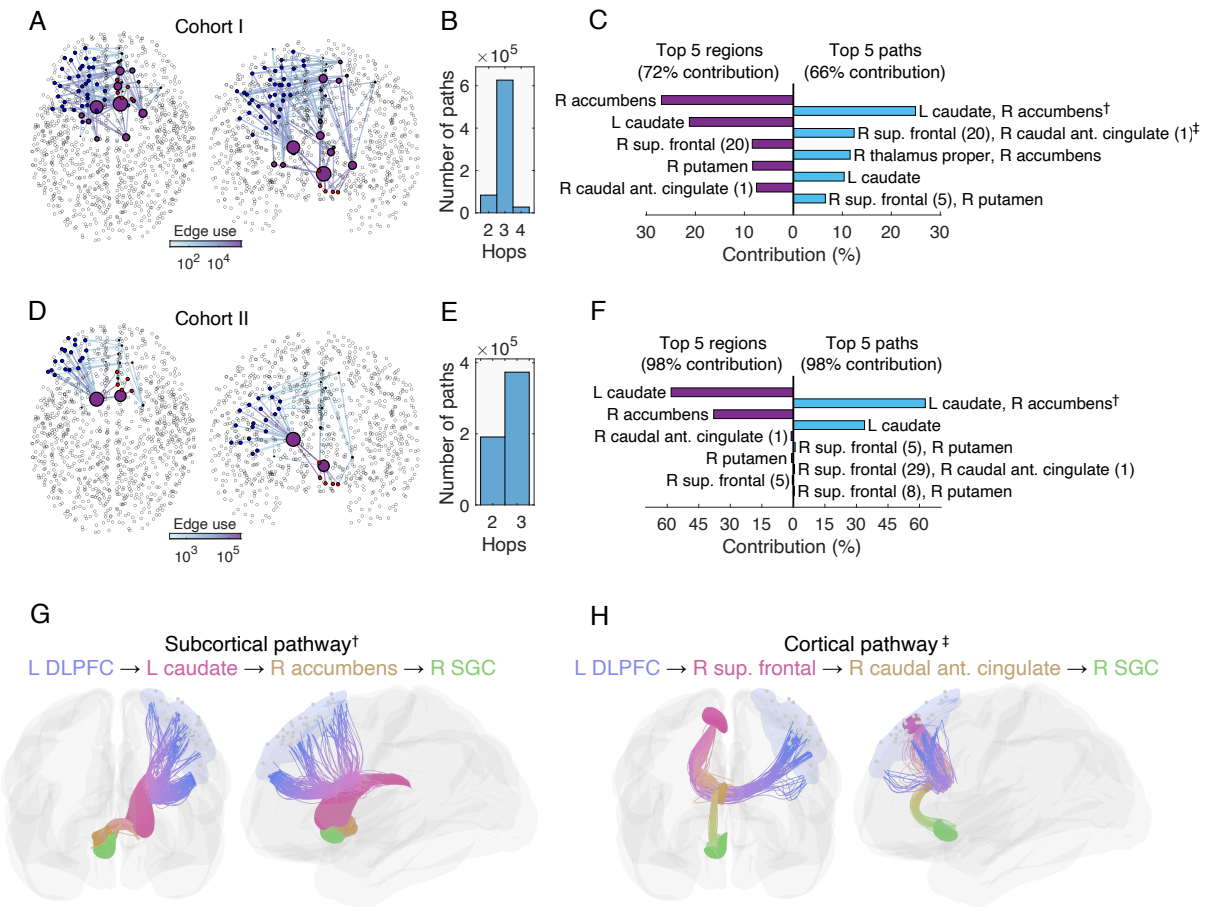

Figure 2. DLPFC-SGC neuroanatomical pathways associated with TMS treatment response. **(A)** Network visualisation of paths originating from stimulated grey matter regions in the left DLPFC (blue), via intermediate regions (purple), to right SGC regions (red), in Cohort I. The size of intermediate regions and colour of connections are proportional to the number of times they are traversed. **(B)** Number of white matter hops from stimulated to SGC regions in Cohort I. **(C)** Top 5 intermediate regions and paths in Cohort I. **(D-F)** Same as (A-B) but in Cohort II. Anatomical visualisations of the **(G)** subcortical and **(H)** cortical pathways from left DLPFC to right SGC reconstructed using tractography. Fibre colours show different white matter hops along the connectome.

How do these neuroanatomical pathways advance on previous work on fMRI-guided TMS for depression? Prior evidence suggests that TMS is more effective when targeted to DLPFC sites with strong negative FC (i.e., anti-correlation) to the SGC [6–8] (although see [3]). As an initial check, we first confirmed this association in both depression cohorts using FC from the normative connectome dataset (Fig S2; cohort I: $r = -0.37$, $p = 0.0366$; cohort II: $r = -0.46$, $p = 0.0102$). We then computed two modalities of DLPFC maps: the first based on the FC to the SGC and second based on the number of hops via white matter pathways to the SGC (Figs S3A,B). We found a positive correlation between the two maps, indicating that DLPFC sites with negative FC to the SGC also tend to be connected to it via shorter, more direct polysynaptic white matter pathways (Fig S3C; $r = 0.85$, $p < 10^{-12}$). This finding provides a neuroanatomical basis explaining the efficacy of state-of-the-art methods for fMRI-guided TMS therapy in depression.

We performed a series of complementary analyses to assess the robustness of our findings. First, we confirmed the relationship between white matter communication and treatment response using leave-one-out tests (Fig S1) and a statistical framework based on surrogate connectomes (Fig S4). Second, we recomputed our analyses using an alternative dataset of normative connectomes, wherein brain networks were mapped by an independent research

group using a different sample of subjects, image acquisition and preprocessing methods, connectivity reconstruction techniques, and grey matter parcellation. Once again, we found that communication via white matter pathways was correlated with symptom improvement in both cohorts (Fig S2; cohort I: $r = -0.43$, $p = 0.0165$; cohort II: $r = -0.40$, $p = 0.0250$) and that DLPFC sites more anti-correlated to the SGC were reachable via fewer white matter hops (Fig S3D-F, $r = 0.73$, $p < 10^{-12}$). Lastly, we note that our analyses used the *shortest path routing* model to identify pathways from the DLPFC to the SGC. We considered a host of alternative network communication models and found that *shortest path routing* was the only model correlated with clinical outcomes across both patient cohorts and both normative connectome datasets (Fig S2).

In sum, we use network communication models to illuminate the neuroanatomical basis of DLPFC-targeted TMS for depression. We show that structurally-constrained communication from stimulation sites at the left DLPFC to the right SGC is correlated with patient outcomes in two independent cohorts. For the first time, we unveil putative cortical and subcortical circuits involved in therapeutic mechanisms. The subcortical pathway, featuring caudate and accumbens nuclei, supports literature implicating fronto-striatal signalling in depression [18,19], while the cortical pathway mediated by the anterior cingulate cortex echoes tract-tracing findings of DLPFC-SGC circuitry in monkeys [10,11]. These results establish the utility of structural connectivity—when coupled with computational models of neural communication and dynamics [20–22]—to inform stimulation protocols based on polysynaptic fibre pathways. A promising prospect is the use of these models to augment current methods based on direct tracts, such as fibre filtering and lesion network mapping [13,15]. In the future, our work could also be extended to evaluate and inform personalised targeting based on each individual's unique connectome [9], across brain stimulation modalities including TMS and deep brain stimulation.

Materials and Methods

Clinical cohorts

We considered two previously published cohorts of individuals with treatment resistant depression who underwent repetitive TMS to the left DLPFC. Cohort I comprised 25 individuals (17 females, age 54.8 ± 9.9) treated at the Berenson-Allen Center at Beth Israel Deaconess Medical Center, Boston, USA [7]. Patients were diagnosed with major depression and met the criteria for medication-resistance, including failure to respond to at least one antidepressant. The treatment consisted of repetitive high-frequency TMS to the left DLPFC (10 and 20 Hz at 110% and 120% of the resting motor threshold, respectively) delivered daily for a period of 4-7 weeks. Precise stimulation sites were determined by moving 5.5 cm anterior to the motor threshold location along a parasagittal line. TMS coordinates were recorded using a neuronavigation system and later transformed to MNI space using the patients' T1-weighted anatomical scans. Treatment response was measured by the change in the self-report of depressive symptoms using the Beck Depression Inventory (BDI-II), assessed on the first and last day of therapy. The mean baseline BDI score of 38.6 ± 9.3 was significantly decreased to 21.2 ± 13.0 following TMS treatment ($p < 0.0001$). Complete details on the clinical characterisation, data acquisition and TMS treatment for Cohort I are reported in [7].

Cohort II contained 24 individuals who completed 5-8 weeks of repetitive TMS to the left DLPFC as part of a larger clinical study (Australian New Zealand Clinical Trials Registry: Investigating Predictors of Response to Transcranial Magnetic Stimulation for the Treatment of Depression; ACTRN12610001071011) [8]. Individuals met the key inclusion criteria of major depression diagnosis and treatment resistant depression at Stage III of the Thase and Rush classification. Repetitive high-frequency TMS was delivered to the left DLPFC at 10 Hz and 110% of the motor threshold. Patient-specific stimulation coordinates were determined using the F3 beam approach and later transformed to MNI space using anatomical scans. Treatment response was measured as the difference in the self-report Montgomery–Åsberg Depression Rating Scale (MADRS) at baseline and 6 weeks after the start of TMS therapy. The mean baseline MADRS score of 33.7 ± 6.7 was significantly at 6 weeks to 24.3 ± 11.4 ($p = 0.0003$). Further details on the patient demographics, data acquisition and TMS treatment for Cohort II are found in [8] and https://www.anzctr.org.au/Trial/Registration/TrialReview.aspx?id=336262.

Normative brain connectivity datasets

We used two previously published and openly available datasets of normative structural and functional connectivity. Normative connectomes—mapped from high-quality brain images of healthy adults—are commonly used to inform clinical brain stimulation studies as they have higher signal-to-noise ratio compared to connectivity reconstructed from patient data [13,23]. As detailed below, we used an established method to generate normative connectomes that mitigates tractography biases and filters out individual-level artefacts [24,25]. These factors contribute to the accurate delineation of white matter fibres and pathways associated with brain stimulation clinical outcomes [13,26].

The first normative dataset, used in all analyses in the main text, comprised brain networks for 70 healthy young adults (mean age 28.8 ± 9.1, 27 women) acquired at the University of Lausanne, Switzerland [27]. Grey matter was parcellated into 1,000 cortical and 14 subcortical (left and right thalamus, caudate, putamen, pallidum, accumbens area, hippocampus and

amygdala) regions [28]. Structural connectivity was estimated from the diffusion MRI of individual participants using deterministic white matter tractography. The strength of the white matter connection between two regions was computed as the number of streamlines intersecting them divided by the average of their surface areas. Resting-state fMRI volumes underwent preprocessing to correct for motion, physiological confounds and global signal. The functional connectivity of each individual was computed as the Pearson correlation between regional time courses of blood oxygenation level dependent (BOLD) signals. Further details on image acquisition and connectivity reconstruction are found in [27].

The second dataset, used in the replication analysis of Fig S2, comprised brain networks from 1,000 Human Connectome Project (HCP) healthy young adults. Details on HCP imaging acquisition and pre-processing are described in [29–31]. Grey matter regions were defined based on the on the Schaefer 800 (7 Networks) parcellation [32] combined with the same 14 subcortical regions listed above. Structural connectivity was computed using probabilistic white matter tractography applied to diffusion MRI, and the strength of the structural connections was inferred as the streamline count between grey matter regions. Functional connectivity was once again computed as the Pearson correlation of regional BOLD time courses following resting-state fMRI preprocessing. Further details on connectivity reconstruction are provided in [33].

We applied an established consensus method to generate group-representative connectomes from the structural connectivity matrices of individual subjects [24]. The method selects the white matter connections most reliably found across individuals, while preserving the sample's average connection density, numbers of intra- and inter-hemispheric connections, and distribution of connection lengths. This approach yields a prototypical map of human brain connectivity that mitigates tractography reconstruction errors, filters out individual-level artifacts, and boosts signal-to-noise ratio [24,25]. For the first dataset, this yielded a 1,014 × 1,014 structural connectivity matrix with 2.3% connection density. For the second dataset, we obtained a 814 × 814 structural connectivity matrix with 27.8% connection density. These group-representative connectomes were used as inputs to network communication models to identify white matter pathways from the DLPFC to the SGC. Finally, the group-level functional connectivity used in Figs S1 and S2 were computed by averaging the functional matrices of participants from each dataset.

Brain network communication models

In the main text, we computed brain network communication using the *shortest path routing*. This model identifies the shortest, most direct channel of communication between two brain regions. For a pair of regions that do not share a direct white matter connection—e.g., the DLPFC and the SGC—the shortest path comprises a sequence of two or more white matter connections via the connectome. We considered the weighted shortest path, such that the length of a path is quantified by taking into account the total strength of the fibres comprising it.

Formally, let W be the structural connectivity matrix, where entry $W(i,j)$ denotes the strength of the white matter connections between regions i and j. We first define the matrix of connection lengths $L = -\log(W)$ to quantify the distance or travel cost between pairs of regions. The shortest path between two regions a and b is the sequence of connections $\Pi(a,b) = \{a, u, \dots, v, b\}$ that minimises the sum $L(a,u) + \cdots + L(v,b)$, known as the shortest path length. The capacity for TMS communication from a to b was defined as the number of hops along their shortest path, such that $H(a,b) = |\Pi(a,b)|$. Computed for every pair of

regions, this yielded the communication matrix H (Fig 1A). In Figure S1, we explored alternative brain network communication models that do not quantify communication via shortest paths. The definitions and technical details of these models can be found in [16,20,34]. The code implementing the network communication models is available in the *Brain Connectivity Toolbox* [35].

Modelling communication from DLPFC TMS sites to the SGC

We computed the average number of white matter hops via the shortest path from TMS sites to the 10-mm radius SGC sphere centred at MNI [6,16,–10]. We first registered TMS coordinates and grey matter parcellations to MNI space. TMS was modelled to activate all grey matter voxels within a 10-mm radius of the stimulation coordinate. Overlaid onto a grey matter parcellation, each TMS coordinate defines a multiset S of voxel parcellation assignments. For example, $S(k) = \{a, a, a, b, b, c, c\}$ denotes that patient k had TMS delivered to 3 voxels assigned to region a, 2 voxels assigned to b and 1 voxel assigned to c. Similarly, the SGC sphere defines a multiset T, which is fixed for all patients. Communication from patient k's TMS site to the SGC was computed as the average number of hops from regions in $S(k)$ to regions in T, weighted by the occurrence of voxel parcellation assignments in both multisets. Formally,

$$h(k) = \frac{1}{|S(k)||T|} \sum_{u \in S(k)} \sum_{v \in T} H(u, v).$$

We note that H is computed on a group-representative connectome, and therefore variations in white matter communication across patients are encoded in $S(k)$ and stem solely from differences in TMS coordinates. In analyses where communication was modelled to loci other than the SGC sphere, the composition of T adjusted accordingly (e.g. Fig 1D,H). In the replication analyses of Fig S2, H was replaced by communication matrices from alternative network models and by functional connectivity matrices. Prominent communication pathways were identified by counting the occurrences of paths from elements in $S(k)$ to elements in T, summed across all patients of the same cohort.

Visualisation

The cortical maps in Fig 1D,H were rendered using *Cerebro* [36]. To visualise the white matter pathways in Fig 2, we first performed tractography on a tissue-unbiased template image of fibre orientation distributions created using multimodal registration [37]. The template was generated in previous work using multimodal registration to guarantee the alignment of white matter tracts with cortical and subcortical grey matter [37]. Streamlines were then transformed to MNI space and visualised using *Cerebro* [36] and *Blender*. All other figures were created using *MATLAB*.

Supplementary Information

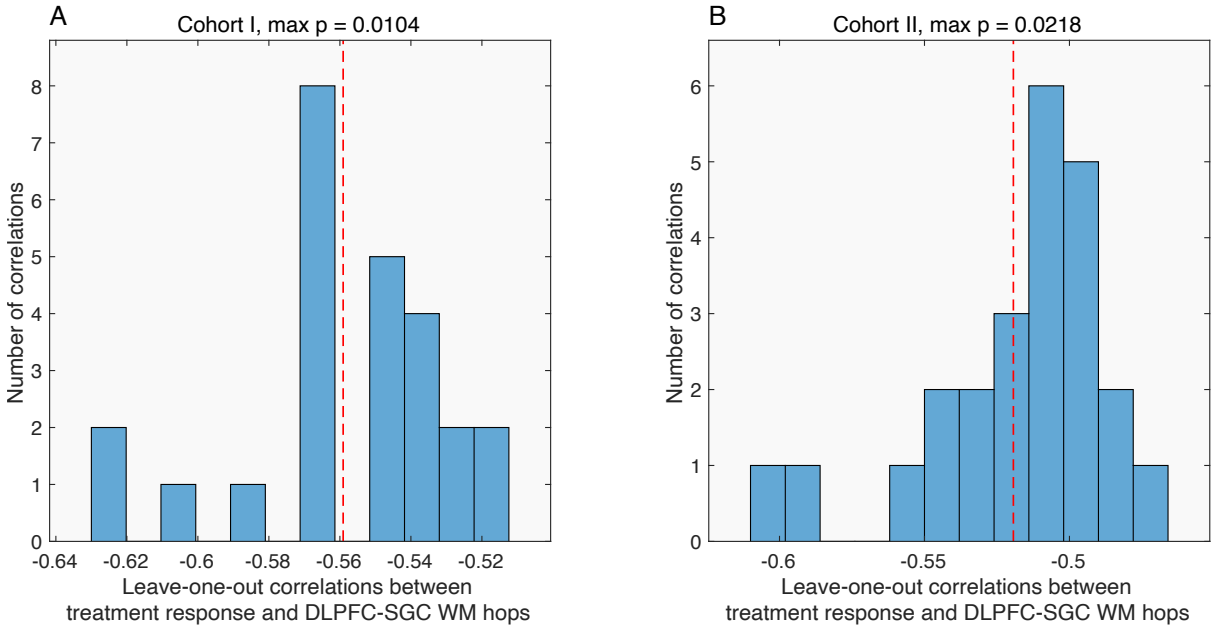

Figure S1. Leave-one-out sensitivity analyses. Correlations between DLPFC-SGC white matter hops and treatment response were computed by leaving out one patient at a time. In both patient cohorts, all leave-one-out correlations were significant (cohort I: Spearman correlation maximum p = 0.0104; cohort II: p = 0.0218), indicating that the associations between white-matter communication and treatment response are not driven by the inclusion/exclusion of any single patient. Dashed red lines show the correlations obtained considering all patients, as reported in the main text analyses.

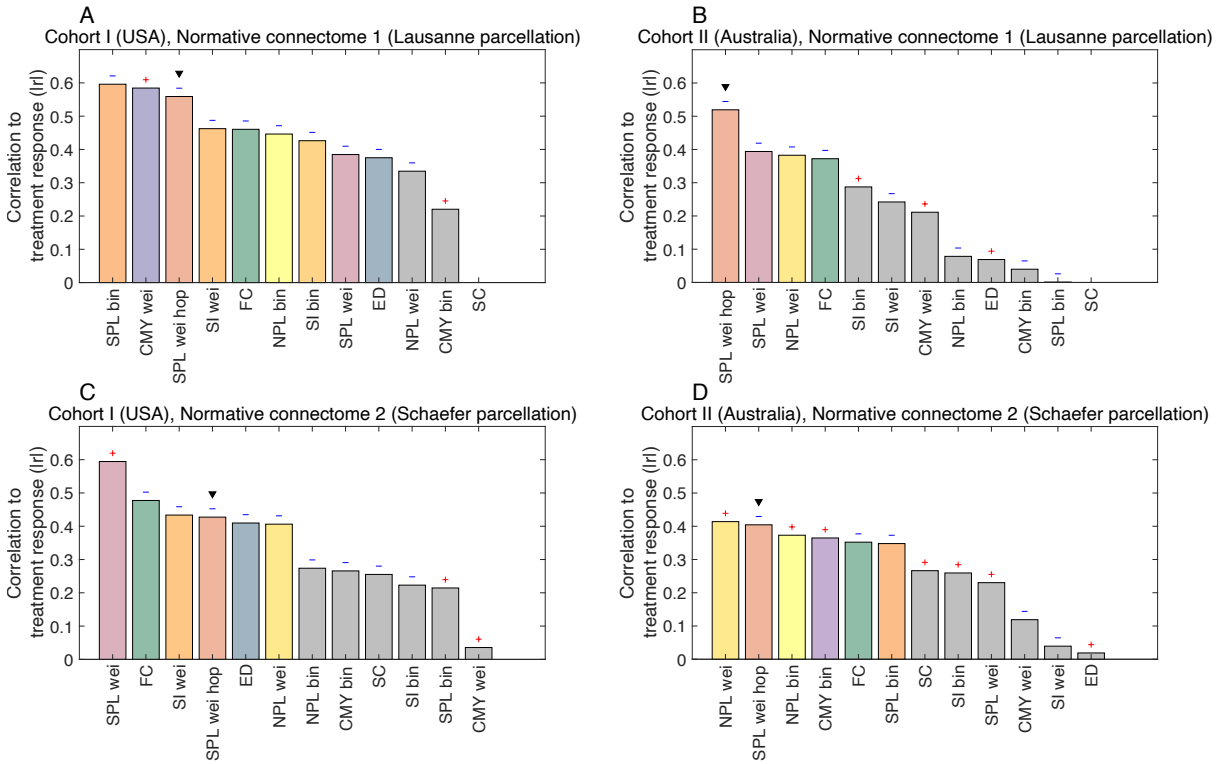

Figure S2. Correlations between treatment response and various connectivity, communication and distance measures. Correlations were computed in two cohorts of patients suffering from depression who received TMS to the left DLPFC and using two normative connectome datasets. All measures capture interactions between the DLPFC stimulation sites and the SGC, and were computed following the method described in *Modelling communication from DLPFC TMS sites to the SGC*. Each coloured bar shows the absolute value of the Spearman correlation coefficient between treatment response and one measure, with signs atop bars indicating the direction

of association. Bars in grey denote correlations that were not significant ($p > 0.05$). Measures include functional connectivity (FC), structural connectivity (SC), Euclidean distance (ED), and multiple network communication measures computed on binary (bin) and weighted (wei) connectomes. Briefly, the network communication measures are the number of hops of the weighted shortest path (SPL wei hop, used in the main text analyses and highlighted by triangular markers), the binary and weighted shortest path lengths (SPL bin, wei), the binary and weighted navigation path lengths (NPL wei, bin), the binary and weighted search information (SI wei, bin), and the binary and weighted communicability (CMY wei, bin). Technical details on these measures are described in [16,20,34].

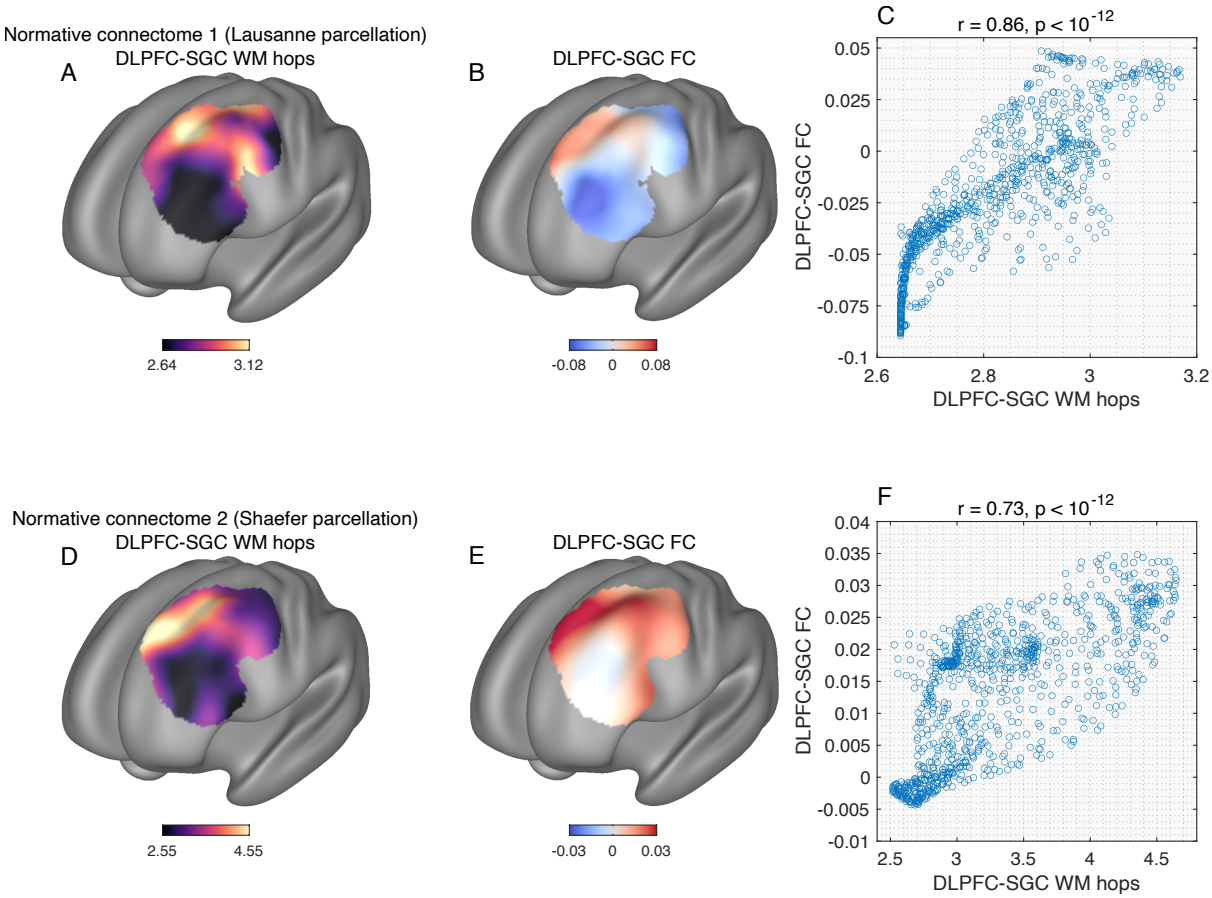

Figure S3. DLPFC maps of the number of white matter hops to the SGC (A,D) and the FC to the SGC (B,E) in two normative connectome datasets. Scatter plots (C,F) show the association between DLPFC-SGC white matter communication and FC. Each dot represents a grey matter voxel in the DLPFC that is accessible to TMS. DLPFC sites functionally anti-correlated to the SGC tend to have shorter, more direct polysynaptic fibre pathways to the SGC (dataset 1: Spearman correlation coefficient $r = 0.86$, dataset 2: $r = 0.73$).

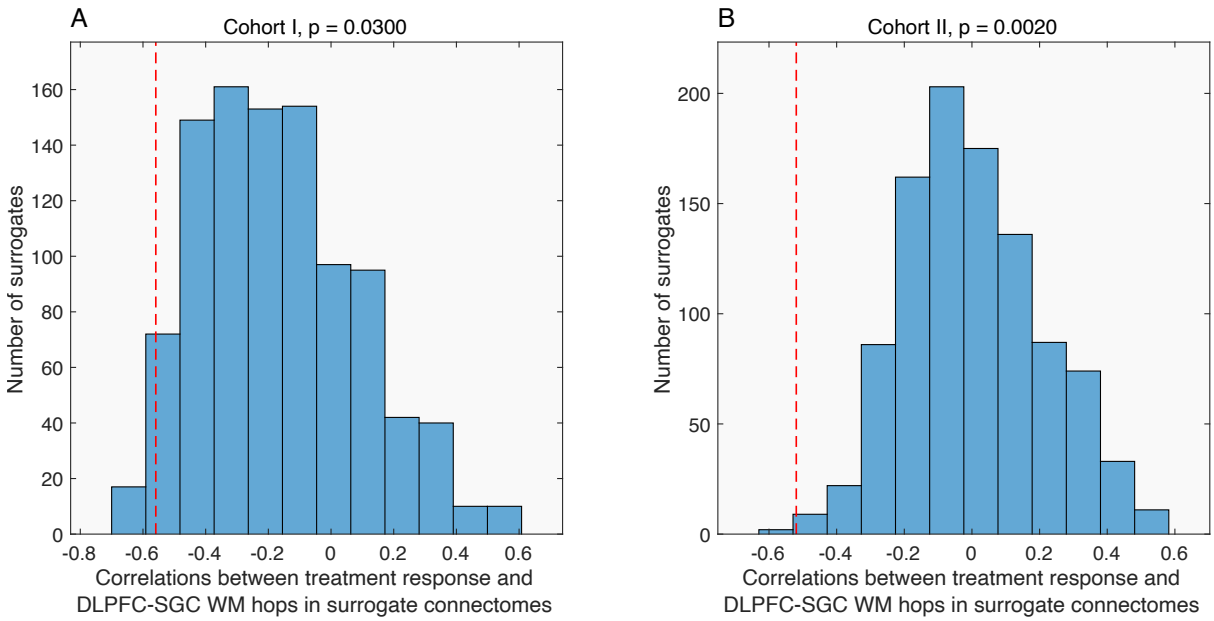

Figure S4. Surrogate connectome analyses. Dashed red lines show the correlations obtained considering empirical connectomes, as reported in the main text analyses. We constructed surrogate connectomes by rewiring connections between brain regions. Surrogate connectomes are brain-like networks that preserve key features of structural connectivity (e.g., the number of tracts intersecting each region, tract length distribution, and the relationship between tract weight and length) but are otherwise randomly shuffled into an alternative realisation of brain wiring [38,39]. We repeated our analyses in an ensemble of 1,000 surrogate connectomes and observed a significant decrease in the association between white matter communication and treatment response (cohort I: non-parametric $p = 0.0300$; cohort II: $p = 0.0020$). This underscores the importance of the detailed topography of human white matter fibres to TMS propagation and its therapeutic efficacy in depression.

References

1. Fitzgerald PB, Brown TL, Marston NAU, Jeff Daskalakis Z, de Castella A, Kulkarni J. Transcranial Magnetic Stimulation in the Treatment of Depression: A Double-blind, Placebo-Controlled Trial. Arch Gen Psychiatry. 2003;60: 1002–1008.

2. Oathes DJ, Zimmerman JP, Duprat R, Japp SS, Scully M, Rosenberg BM, et al. Resting fMRI-guided TMS results in subcortical and brain network modulation indexed by interleaved TMS/fMRI. Exp Brain Res. 2021;239: 1165–1178.

3. Duprat RJ, Linn KA, Satterthwaite TD, Sheline YI, Liang X, Bagdon G, et al. Resting fMRI-guided TMS evokes subgenual anterior cingulate response in depression. NeuroImage. 2025;305: 120963.

4. Tik M, Woletz W, Schuler AL, Vasileiadi W, Cash RFH, Zalesky A, Lamm C, Windischberger C. Acute TMS/fMRI response explains offline TMS network effects – An interleaved TMS-fMRI study. NeuroImage. 2023;267: 119833.

5. Trapp NT, Liu X, Li Z, Bruss J, Keller CJ, Boes AD, et al. Dorsolateral prefrontal cortex TMS evokes responses in the subgenual anterior cingulate cortex: Evidence from human intracranial EEG. bioRxiv. 2024. p. 2024.12.20.629857. doi:10.1101/2024.12.20.629857

6. Fox MD, Buckner RL, White MP, Greicius MD, Pascual-Leone A. Efficacy of transcranial magnetic stimulation targets for depression is related to intrinsic functional connectivity with the subgenual cingulate. Biol Psychiatry. 2012;72: 595–603.

7. Weigand A, Horn A, Caballero R, Cooke D, Stern AP, Taylor SF, et al. Prospective Validation That Subgenual Connectivity Predicts Antidepressant Efficacy of Transcranial Magnetic Stimulation Sites. Biol Psychiatry. 2018;84: 28–37.

8. Cash RFH, Zalesky A, Thomson RH, Tian Y, Cocchi L, Fitzgerald PB. Subgenual Functional Connectivity Predicts Antidepressant Treatment Response to Transcranial Magnetic Stimulation: Independent Validation and Evaluation of Personalization. Biol Psychiatry. 2019;86: e5–e7.

9. Cash RFH, Cocchi L, Lv J, Fitzgerald PB, Zalesky A. Functional Magnetic Resonance Imaging-Guided Personalization of Transcranial Magnetic Stimulation Treatment for Depression. JAMA Psychiatry. 2021;78: 337–339.

10. Joyce MKP, García-Cabezas MÁ, John YJ, Barbas H. Serial Prefrontal Pathways Are Positioned to Balance Cognition and Emotion in Primates. J Neurosci. 2020;40: 8306–8328.

11. Joyce MKP, Barbas H. Cortical Connections Position Primate Area 25 as a Keystone for Interoception, Emotion, and Memory. J Neurosci. 2018;38: 1677–1698.

12. Cash RFH, Zalesky A. Personalized and Circuit-Based Transcranial Magnetic Stimulation: Evidence, Controversies, and Opportunities. Biol Psychiatry. 2024;95: 510–522.

13. Hollunder B, Ostrem JL, Sahin IA, Rajamani N, Oxenford S, Butenko K, et al. Mapping dysfunctional circuits in the frontal cortex using deep brain stimulation. Nat Neurosci.

2024;27: 573–586.

14. Sydnor VJ, Cieslak M, Duprat R, Deluisi J, Flounders MW, Long H, et al. Cortical-subcortical structural connections support transcranial magnetic stimulation engagement of the amygdala. Science Advances. 2022 [cited 11 Jan 2025]. doi:10.1126/sciadv.abn5803

15. Siddiqi SH, Kording KP, Parvizi J, Fox MD. Causal mapping of human brain function. Nat Rev Neurosci. 2022;23: 361–375.

16. Seguin C, Sporns O, Zalesky A. Brain network communication: concepts, models and applications. Nat Rev Neurosci. 2023;24: 557–574.

17. Avena-Koenigsberger A, Misic B, Sporns O. Communication dynamics in complex brain networks. Nat Rev Neurosci. 2018;19: 17–33.

18. Price JL, Drevets WC. Neurocircuitry of Mood Disorders. Neuropsychopharmacology. 2009;35: 192–216.

19. Pizzagalli DA, Holmes AJ, Dillon DG, Goetz EL, Birk JL, Bogdan R, et al. Reduced caudate and nucleus accumbens response to rewards in unmedicated individuals with major depressive disorder. The American journal of psychiatry. 2009;166. doi:10.1176/appi.ajp.2008.08081201

20. Seguin C, Jedynak M, David O, Mansour S, Sporns O, Zalesky A. Communication dynamics in the human connectome shape the cortex-wide propagation of direct electrical stimulation. Neuron. 2023. doi:10.1016/j.neuron.2023.01.027

21. Menardi A, Momi D, Vallesi A, Barabási A-L, Towlson EK, Santarnecchi E. Maximizing brain networks engagement via individualized connectome-wide target search. Brain Stimul. 2022;15: 1418–1431.

22. Momi D, Wang Z, Griffiths JD. TMS-evoked responses are driven by recurrent large-scale network dynamics. Elife. 2023;12. doi:10.7554/eLife.83232

23. Wang Q, Akram H, Muthuraman M, Gonzalez-Escamilla G, Sheth SA, Oxenford S, et al. Normative vs. patient-specific brain connectivity in deep brain stimulation. Neuroimage. 2021;224: 117307.

24. Betzel RF, Griffa A, Hagmann P, Mišić B. Distance-dependent consensus thresholds for generating group-representative structural brain networks. Netw Neurosci. 2019;3: 475–496.

25. Roberts JA, Perry A, Roberts G, Mitchell PB, Breakspear M. Consistency-based thresholding of the human connectome. Neuroimage. 2017;145: 118–129.

26. Horn A, Al-Fatly B, Neumann WJ, Neudorfer C. Connectomic DBS: An introduction. Connectomic Deep Brain Stimulation. Academic Press; 2022. pp. 3–23.

27. Griffa A, Alemán-Gómez Y, Hagmann P. Structural and functional connectome from 70 young healthy adults. [cited 29 Jan 2025]. doi:10.5281/zenodo.2872624

28. Cammoun L, Gigandet X, Meskaldji D, Thiran JP, Sporns O, Do KQ, et al. Mapping the human connectome at multiple scales with diffusion spectrum MRI. Journal of Neuroscience Methods. 2012;203: 386–397.

29. Glasser MF, Sotiropoulos SN, Wilson JA, Coalson TS, Fischl B, Andersson JL, et al. The minimal preprocessing pipelines for the Human Connectome Project. Neuroimage. 2013;80: 105–124.

30. Sotiropoulos SN, Jbabdi S, Xu J, Andersson JL, Moeller S, Auerbach EJ, et al. Advances in diffusion MRI acquisition and processing in the Human Connectome Project. Neuroimage. 2013;80: 125–143.

31. Smith SM, Beckmann CF, Andersson J, Auerbach EJ, Bijsterbosch J, Douaud G, et al. Resting-state fMRI in the Human Connectome Project. Neuroimage. 2013;80: 144–168.

32. Schaefer A, Kong R, Gordon EM, Laumann TO, Zuo X-N, Holmes AJ, et al. Local-Global Parcellation of the Human Cerebral Cortex from Intrinsic Functional Connectivity MRI. Cereb Cortex. 2018;28: 3095–3114.

33. Mansour L S, Tian Y, Yeo BTT, Cropley V, Zalesky A. High-resolution connectomic fingerprints: Mapping neural identity and behavior. Neuroimage. 2021;229: 117695.

34. Zamani Esfahlani F, Faskowitz J, Slack J, Mišić B, Betzel RF. Local structure-function relationships in human brain networks across the lifespan. Nature Communications. 2022;13: 1–16.

35. Rubinov M, Sporns O. Complex network measures of brain connectivity: uses and interpretations. Neuroimage. 2010;52: 1059–1069.

36. Mansour L S. Cerebro_Viewer A Pythonic 3D viewer to visualize and plot brains. [cited 4 Feb 2025]. doi:10.5281/zenodo.7885669

37. Lv J, Zeng R, Ho MP, D'Souza A, Calamante F. Building a tissue-unbiased brain template of fiber orientation distribution and tractography with multimodal registration. Magn Reson Med. 2023;89: 1207–1220.

38. Váša F, Mišić B. Null models in network neuroscience. Nat Rev Neurosci. 2022;23: 493–504.

39. Betzel RF, Bassett DS. Specificity and robustness of long-distance connections in weighted, interareal connectomes. Proc Natl Acad Sci U S A. 2018;115: E4880–E4889.

Author disclosure

L.C., R.F.H. and A.Z. are involved in a not-for-profit clinical neuromodulation centre (Queensland Neurostimulation Centre) that offers neuroimaging-guided neurotherapeutics. In the last 3 years P.B.F. has received reimbursement for educational activities from Otsuka Australia Pharmaceutical Pty Ltd and equipment for research from Brainsway Ltd.